https://doi.org/10.22226/2410-3535-2023-2-143-148

Evolution of an approach to the modeling of zirconium hydrides morphology based on Monte-Carlo method in 3D representation

T. N. Aliev, M. Yu. Kolesnik†

†kolesnik.mikhail@gmail.com

Lebedev Physical Institute of the RAS, Moscow, 119991, Russia

The paper describes a new computational module which simulates the zirconium hydride morphology in 3D representation. Hydrides are assumed to be discs with two possible orientations in perpendicular planes. We describe nucleation based on the classical theory of the heterogeneous nucleation on crystal lattice defects. Spatial and energy distributions of the defects can be predefined based on microstructural data. To describe the growth of zirconium hydrides and "competition" between them as sinks for hydrogen, we apply Voronoi tessellation of hydride centers. The growth of any hydride is provided by hydrogen from its Voronoi cell. Serial calculations allow us to obtain statistical parameters (mean and variance) based on Monte-Carlo method for any morphology metrics.

Keywords: hydrogen embrittlement, zirconium, hydrides, brittle fracture, ductile fracture, plasticity.

1. Introduction

The hydride precipitation in zirconium is the object under study for a long time [1–3]. Significant interest in this subject arises from the hydrogen embrittlement problem of zirconium-based alloys, which are used as materials for fuel assemble elements in water-cooled nuclear reactors. Hydrogen is a secondary product of water corrosion continuously produced during routine operation, and a part of it can penetrate into zirconium claddings of fuel rods or other structural elements. The zirconium hydride phase precipitation (mainly, stable fcc δ-phase $ZrH_{1.6}$ in considered conditions [4–6]) leads to the degradation of mechanical properties of fuel rod claddings [7–9], namely, to the reduction of ductility, fracture toughness and ultimate strain. The degree of hydrogen embrittlement depends on the volume fraction of hydrides and their morphology which is understood as a set of such parameters as hydride size, inter-hydride distance and orientation to the external stress [10–12]. Moreover, the ductile to brittle transition of the fracture mode is determined not only by mean values of morphology parameters, but also by their distribution function. For instance, the probability of brittle fracture can depend on the probability of a hydride with appropriate orientation to be longer than the critical length in the material yield area [12].

The study of zirconium hydride morphology was pursued for long time with optical and electron microscopes. It was revealed that micro hydrides had the form of flattened needles ("sword-shaped" [13]) with length up to few hundreds of nanometers. An array of microscopic hydrides from ordered structures or macro hydrides [14,15] is also known as a stack [16,17]. Stacks have dendrite-like structure and look like branched undulating surfaces [18]. The size of macro hydrides ranges from tens to hundreds of micrometers and many times exceeds the grain size in industrial zirconium alloys [14,18,19].

Theoretical models simulating the morphology of macrohydrides in zirconium developed for practical applications are based on semi-correlation dependencies [20–22] or a numerical solution of differential equation systems [23–27]. All these models can simulate only some of mean parameters of hydride morphology in 2D representation. The most popular parameter for simulation is radial hydride fraction (RHF) in zirconium fuel rod claddings. In addition, models proposed in [25] and [26] can predict the mean hydride length and mean inter-hydride distance.

Previously, we developed an approach [28] for modeling of all second phase precipitates morphology parameters in a 3D representation including the estimation of statistic morphology parameters based on Monte Carlo method. For example, it allows for a given thermo-mechanical load scenario to estimate the probability that hydride connectivity will be below the threshold value corresponding to the critical local embrittlement. In this article, we further develop this approach and broaden the model validation with experimental data. Modernization of the model made it possible to take into account the influence of external stresses on the orientation of hydrides and the influence of neighboring hydrides on growth of each other.

Traditionally, hydride morphology in zirconium alloys was studied in a 2D representation analyzing micrographs, and the understanding of hydrides as extended objects on a plane is dominant in previously published models. However, recently the authors of hydride morphology analysis package HAPPy [29] claimed, that they would continue the development of their package to analyze 3D images which can be obtained by means of X-ray tomography [18]. Numerical analysis of such structures will definitely need the development of new morphology metrics characterizing 3D

objects and theoretical models for simulation of hydride's morphology in 3D representation. The approach presented in [28] and developed in this article is the first one predicting statistical parameters of 3D hydride morphology in simple and, at the same time, general approximation with low computational costs.

2. The model description

The detailed model description was previously published in [28]; here we present only an outline of the model and its modernization (in the next section). We simulate the zirconium hydride nucleation in classical heterogeneous approximation at prescribed nucleation sites. Before the total simulation, the user describes the spatial distribution of crystal defects serving as nucleation sites; the energy of every defect is a stochastic value with a given probability density distribution of the defect energy. Both the space and energy distributions of defects are technically arbitrary, but should ideally be given based on the microstructural data about the nature of the defects serving as nucleation sites. We assumed a uniform spatial distribution in a cubic lattice and a normal distribution of the defect energy probability density (the mean is 8 eV, the variance is 0.33, according to [28]). For every nucleation site (point defect) at every time step τ the hydride nucleation probability is estimated as $R \cdot \tau$, where R is the nucleation frequency, which, according to the classical heterogeneous nucleation theory [30, 31], is equal to

$$R = Zj_{\text{n}} \cdot \exp(-\Delta G^* / kT), \qquad (1)$$

where j_{n} is the diffusion flow to the nucleus, Z is Zeldovich factor, k is Boltzmann constant, T is temperature, ΔG^* is Gibbs free energy change during the nucleation of critical nucleus, which has the form:

$$\Delta G^*(d^*) = \Omega^*(g_{\text{mech}} - \Delta\mu / v_{\text{H}}) + S^*\gamma - G_{\text{d}}, \qquad (2)$$

Ω^*, S^* are volume and surface area of the critical nucleus with the diameter d^*, γ is specific surface energy of the interphace, $\Delta\mu = X_{\text{a}} kT \cdot \ln(C_{\text{s}}/C_{\text{e}})$ — the chemical potential change during the phase transition, where C_{s} is local hydrogen concentration dissolved in the metal matrix, C_{e} is equilibrium concentration for precipitation, $X_{\text{a}} = 0.62$ — molar fraction of hydrogen in hydride δ-phase $ZrH_{1.6}$, v_{H} is hydrogen atomic volume in hydride, $g_{\text{mech}} \approx \sigma_{\text{Y}}\varepsilon$ — mechanical energy per unit volume, where σ_{Y} is yield stress, ε is volume dilatation due to the phase transition ($\varepsilon \approx 0.17$ for α-Zr$\rightarrow$ δ-$ZrH_{1.6}$, [32]), G_{d} is the defect energy. The probability of the hydride nucleation depends on the defect energy G_{d} and the local concentration of dissolved hydrogen C_{s} (the last factor was ignored in [28]).

Hydride growth is supported be the diffusion sink from the solid solution. The hydrogen flux was written as a flow to the disk edge having consideration for self-stresses [33]:

$$j = 2\pi^2 D_{\text{H}} d \cdot \frac{C_s - C_e \cdot \exp\left(-A\dfrac{\sigma_{\text{Y}} v_{\text{H}} \varepsilon}{kT}\right)}{\ln\left(R_{\max}/R_{\min}\right) + A\dfrac{\sigma_{\text{Y}} v_{\text{H}} \varepsilon}{kT}}, \qquad (3)$$

D_{H} is hydrogen diffusion coefficient, d is hydride diameter, $A = \pi(1+\upsilon)/4$, where υ — Poisson coefficient, $R_{\max}$, $R_{\min}$ are large and small cutoff radii of the diffusion task; $R_{\min}$ is the maximum of the inclusion's thickness and plastic zone size near the hydride edge $r_{\text{pz}} = Sh\varepsilon / (9\pi A\sigma) \cdot (1+\upsilon) / (1-\upsilon)$, where S is shear modulus; $R_{\max}$ is the minimum of two values: the mean inter-hydride half distance and the distance at which the nearest neighbor hydride perturbs the diffusion field $r_{\max} = 0.5 \cdot hC_{\delta} / (C_{\text{s}} - C_{\text{e}} \cdot (-A\sigma_{\text{Y}} v\varepsilon / kT))$, where C_{δ} is hydrogen concentration in δ-phase $ZrH_{1.6}$.

2.1. The model's modernization

The first feature we have added to our computational module was the account of the external stresses influence on the orientation of zirconium hydrides, which is crucial for the practical application. We consider here only two perpendicular orientations of hydrides (radial and tangential regarding the geometry of fuel rod cladding), ignoring the third possible perpendicular orientation. This is because of considering the industrial zirconium alloys with the predefined texture and typical mechanical loading. Hydrides in zirconium fuel rod cladding in the absence of external stress are precipitate mainly in tangential direction. During its lifetime, fuel rod cladding experiences hoop stresses mostly. Hoop tension during the dry storage of spent nuclear fuel contributes to increase of the radial hydride fraction. The fraction of hydrides in the third perpendicular direction ("axial" hydrides in fuel rod cladding) is low due to the weak axial tension and texture factor. Kearns factor favoring the axial hydrides is around 0.13 in Zircaloy-4 [21] and 0.045 in Zircaloy-2 [34].

The fraction of radially oriented hydrides F_{r} is usually estimated following the semi-correlation dependence [35, 20, 21, 23, 36]:

$$F_r = \frac{1 - f_{\text{tex}}}{1 + f_0 \exp\left(-\sigma\Omega / kT\right)} + f_{\text{tex}}, \qquad (4)$$

σ is tangential tension, f_{tex} is textural factor, which can be evaluated based on the pole figures analysis or Kearn's factors [36], Ω, f_0 — the model parameter (susceptibility to stress and microstructural factor). The model parameters Ω and f_0 are usually estimated by comparison with "reorientation curve" (experimental dependence of F_{r} on σ) and can vary for different alloys. The type of Eq. (4) can be easily derived as a ratio of nucleation frequencies of radially-oriented hydrides to the sum of radially-oriented and tangentially-oriented ones [36]. Therefore, we apply Eq. (4) in our model, however with a little different interpretation. We consider F_{r} as a probability of nucleated hydride to be radial and $(1-F_{\text{r}})$ as a probability of the hydride to be tangential. Once nucleated, hydrides do not change their orientation. The short validation of the Eq. (4) can be seen in supplementary material (Appendix A).

The second important feature which we added to our computation module was the account of mutual influence of hydrides on the growth of nearest neighbours (can be interpreted as a competition for dissolved hydrogen). Diffusion flux of hydrogen in the form of Eq. (3) corresponds to the isolated hydride, which growth does not affect by other hydrides. However, the distance between hydrides is a stochastic value and some hydrides can be close to each

other, and they will "compete" as sinks for the hydrogen flux from the solid solution. Hydride which is far from others, in contrast, will be the only sink and will grow as an isolated hydride following the Eq. (3). The hydrides clustering influence not only growth, but nucleation of new hydrides as well. Supersaturation in the vicinity of the hydride cluster is lower than far from it, thus the nucleation probability is higher far from hydrides than in the vicinity of them.

The modernization of the model made it possible to take into account the clustering effect. It is based on the approximation avoiding significant computational costs. The main idea is that the computational domain is tessellated into Voronoi cells, with vertices in centers of hydrides. The Voronoi cell of the given vertex is the region consisting of all points closer to this vertex than to any other (the current implementation ignores the hydride size and vertices of the Voronoi diagram are centers of hydrides). If a new hydride nucleates, the algorithm retessellates the domain and add the new Voronoi cell at the expense of rebuilding the neighbor cells. Hydrogen concentration remains the same in all old cells (including rebuilt ones), while in a new one the hydrogen content follows the total hydrogen amount conservation. For more details and illustrations see in supplementary material (Appendix B).

The simplified approach for hydride growth modeling is based on the change of accurate solution of the diffusion task by assumption that each hydride captures hydrogen only from its own Voronoi cell. Thus, the amount of hydrogen which can be captured by the hydride (consequently, the size of the hydride) is defined by the volume of its Voronoi cell, if new hydrides did not nucleate and the cell was not rebuilt.

3. Application of the approach

3.1. Numerical evaluation of the zirconium hydride clustering effect

We performed a few series of mass calculations to compare the results calculated with the new and old versions of the model to estimate the effect of modernization. The modelling temperature scenario was chosen as a typical one for laboratory experiments on hydride morphology study in zirconium alloys. We assumed cooling of samples hydrogenated up to 200 ppm from 330 to 260°C with cooling rate 20°C/min. These conditions lead to a precipitation of small hydrides and corresponded to the application scope of the approach.

Totally, we performed three series of mass calculations. Each series included six hundred independent calculations of the same numerical experiment. As a result of these calculations, we got histograms of hydride size, radial hydride length density (RHLD) and hydride continuity coefficient (HCC); further, we elucidated parameters of normal distribution for these morphology metrics analyzing their histograms: mathematical mean and variance (Monte Carlo method). Radial hydride length density (RHLD) is the sum of the length of radially-oriented hydrides per a unit area, it was applied as a hydride morphology metric characterizing the hydrogen embrittlement degree in [37,38]. Hydride continuity coefficient (HCC) is defined as a summary length of hydride projections in a band with width 100 μm divided by the length of the band [39]. The width of the band can vary; for example, in [10] the HCC was defined through the width of band equal to 110 μm. Another known analog of HCC is accumulated hydride length (AHL) applied in [40]. Both metrics demonstrate a strong correlation with hydrogen embrittlement degree [10,40,41].

Zirconium hydride size distribution functions estimated by Monte Carlo method applying models before and after modernization are shown in Fig. 1. The mathematical mean of hydride radius (maximum of the distribution function) decreased after modernization, while the variance increased for few times. This result is expected as we added a new stochastic factor limiting the hydride size — its Voronoi cell volume.

The statistical distribution of the RHLD metric is shown in Fig. 2. The modernization of the model has a little effect on the RHLD: the mean RHLD has moved to higher values, and the distribution width became narrower.

HCC metric distribution is shown in Fig. 3. Band width where HCC defined was 100 μm, while the length of the band had two values: 1 and 3 mm. The effect of modernization is weak for both variants, however for band length 3 mm a little more pronounced. Note that HCC shift after modernization

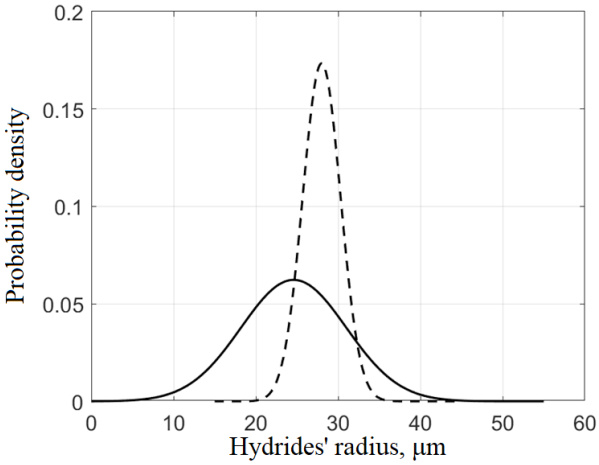

Fig. 1. Zirconium hydride radius distribution. Solid — after modernization, dotted — before modernization.

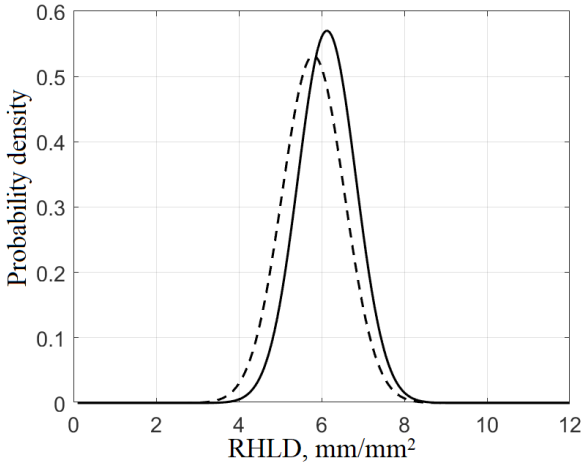

Fig. 2. RHLD distribution. Solid — after modernization, dotted — before modernization.

is to the higher values corresponding to higher hydrogen embrittlement degree. Therefore, modernization of the model reduced excessive optimism of the previous model version.

An important parameter influencing the fracture brittleness of hydrogenated zirconium is hydride cluster length, which is defined as the length of continuous hydride projection onto a given direction in a band having 100 μm width (by analogy with HCC). Before modernization the hydride cluster length had distribution as a sum of normal distributions corresponding to clusters having one, two, three and so on hydrides (see Fig. 4). The modernization changes significantly the overall picture as distribution for each group of clusters becomes wider and shifts to lower values (see Fig. 1). Moreover, the more hydrides in the cluster, the greater will be the shift. That is the consequence of the mutual influence of hydrides on growth of neighbors. As a result, the total cluster length distribution can be approximated by only one normal distribution with a good accuracy, see Fig. 4.

3.2. Model validation with experimental data

The experiment described in [42] was chosen for the simulation and validation of the model, since the samples used there contained a small amount of hydrogen and had small hydrides with a low number of intersections. Specifically, a dog-bone tensile sample E1 in [42] was made of Zr-2.5Nb alloy and contained 55 ± 3 ppm of hydrogen. It was subjected to a thermal cycle with the maximum temperature of 400°C followed by cooling to room temperature under the external tension equal to 225 MPa. Note that, according to micrographs from [42], the radial hydride fraction is around 0.5, which differs from the data of [20] where radial hydride fraction was around 1 at 225 MPa in Zr-2.5Nb (see Fig. S1, supplementary materials). We are concentrated here on the investigation of spatial and statistical distribution of hydride morphology metrics and will postulate the radial hydride fraction 0.5 in simulation of E1 specimen.

The hydride length distribution in E1 sample has been estimated based on micrograph Fig. 2 d in [42]. Then, we compared it with the values calculated for the same conditions by our model before and after modernization. The results are shown in Fig. 5. The mean value of hydride length (the distribution function maximum) coincides; however, the experimental histogram is wider than the calculated functions. The model after modernization is consistent with experiments much better and satisfactory.

The simulation and comparison with experimental data was performed as well for other samples E2, L1 and L2 from [42] similarly to E1 sample. Specimens E1 and E2 correspond to the normal manufacturing process of CANDU rod cladding, while L1 and L2 correspond to an alternative manufacturing route, which replaced the cold drawing stage by pilger-type

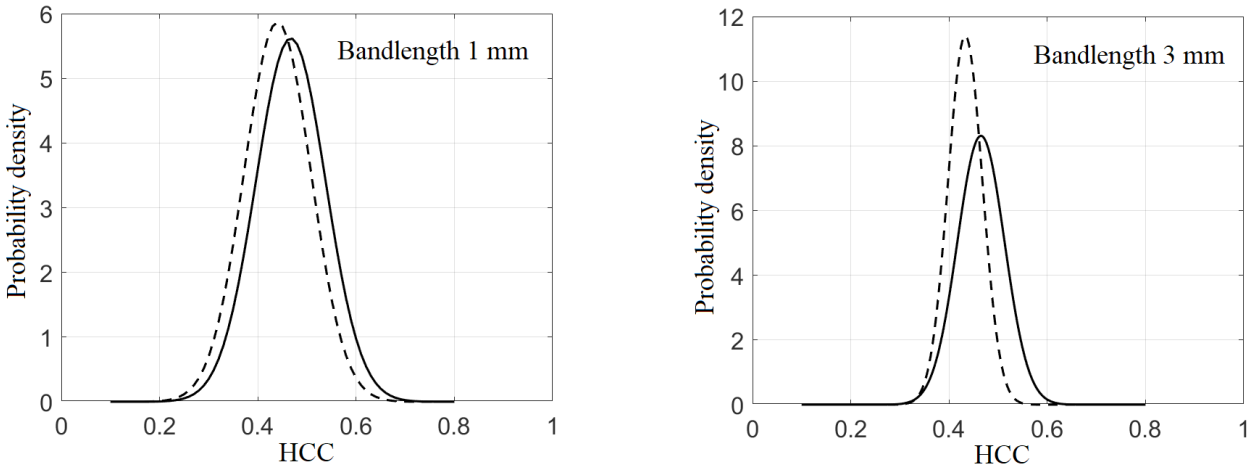

Fig. 3. HCC distribution. Solid — after modernization, dotted — before modernization.

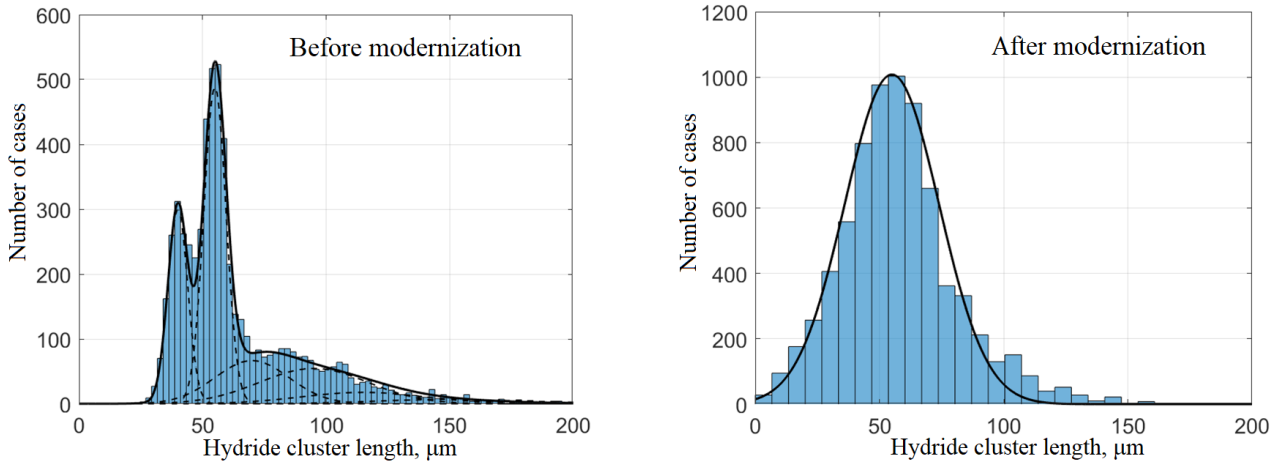

Fig. 4. Zirconium hydride cluster length distribution before and after modernization.

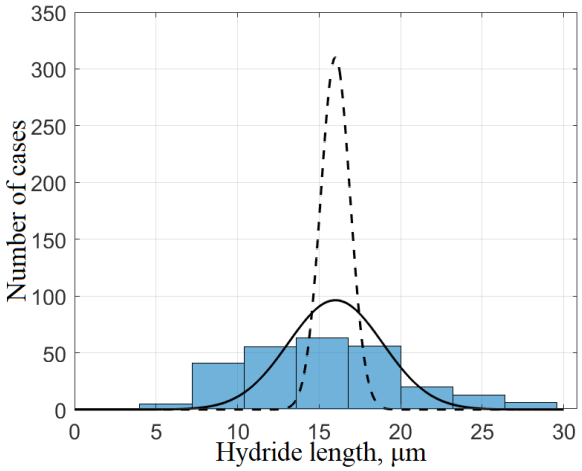

Fig. 5. Zirconium hydride length distribution in the E1 sample used in [42]. Histogram — estimated based on experimental data [42] (Fig. 2 d in [42]), solid line — after modernization, dotted line — before modernization.

cold rolling stage. Nevertheless, the initial microstructure of samples in both cases was similar. Another difference between the samples was the hydrogen content which was varied in the range 44 –130 ppm. Since the hydrogen content determines the precipitation temperature and, therefore, the diffusion coefficient influencing the nucleation process, the hydrogen content variation is in a certain sense similar to the variation in the cooling rate with the same hydrogen content. As results of mass serial calculations, we estimated the statistical parameters of hydride length and HCC distributions for each sample from [42]. The hydride length distribution and HCC value were also estimated from the images of samples' micrographs in [42]. Experimental HCC value was calculated applying the freely available image processing program [43]. Calculation-to-experiment comparison is summarized in Table 1. The agreement for hydride length distribution is satisfactory. HCC value is close to 1 for all samples, which is consistent with calculations as well.

4. Other morphology metrics estimation

To assess the degree of hydrogen embrittlement, various morphology metrics demonstrating correlation with mechanical properties are commonly used in practice. The examples are radial hydride continuity coefficient (RHCF, the maximum projection length of a continuous hydride in a bandwidth 150 μm on the radial direction in the cross-section of cladding tube) [12], radial hydride continuous path (RHCP, characterizes the fracture energy ratio of specimens with and without hydrides) [43] and others. The current approach allows one to estimate any hydride morphology metric on the cross-section of the 3D computational domain as is usually done for micrographs in experiments, which we demonstrate in supplementary materials (Appendix C). For this purpose, we performed 200 independent simulation of 3D domain with sizes $0.3\times0.2\times0.1$ mm modeling the L2 specimen from [42]. In every simulation we numerically analyzed the cross-section 0.3×0.2 mm of the domain at the half height in the end of the simulation applying the tool described in [43].

5. Conclusion

The hydride morphology model simulates nucleation and growth of zirconium hydrides during cooling. It is able to predict both mean value and statistical distribution of any morphology parameter for a specimen with a given size, including:

- hydride length;
- hydride cluster length;
- radial hydride fraction (RHF);
- radial hydride length density (RHLD);
- hydride continuity coefficient (HCC) also known as accumulated hydride length (AHL);
- radial hydride continuously coefficient (RHCF);
- radial hydride continuous path (RHCP).

We carried out a major modernization of the computational module simulating morphology of zirconium hydrides in 3D representation. The main idea of the modernization is Voronoi tessellation of the computational domain containing hydrides. The growth of hydrides is determined in steady-state analytical approximation, assuming each hydride can pick up hydrogen only from its own Voronoi cell. This approach is valid for the nucleation stage, which determines the volume density and spatial distribution of hydrides.

The computational module was validated with experimental data; the modernization leads to a significant effect on computation of hydride length and cluster length distributions. The current approach predicts the probability to find the hydride cluster above the critical size in the area of plastic deformation and, thus, the probability of ductile-to-brittle transition, based on the theory of a weak unit [45].

Supplementary material. *The online version of this paper contains supplementary material available free of charge at the journal's website (lettersonmaterials.com).*

Acknowledgments. The reported study was funded by the Russian Foundation for Basic Research, project #19-32-60031.

Table 1. Calculation-to-experiment comparison. Experimental data were estimated based on experimental data [42].

	H, ppm	T_{pre}*, °C	Length, exp.		Length, calc., old		Length, calc. new		HCC exp.	HCC, calc. old		HCC, calc. new	
			mean	var.	mean	var.	mean	var.		mean	var.**	mean	var.**
E1	55 ± 3	230	15	4.5	16	1	16	2.9	0.93	0.73	0.08	0.85	0.07
E2	67 ± 5	244	15	4	19	3	20	7	0.89	0.71	0.14	0.75	0.15
L1	44 ± 3	214	16	4.5	12.7	0.8	11.5	1.7	0.97	0.84	0.05	0.9	0.05
L2	130 ± 5	299	40	15	78	20	70	25	0.93	0.96	0.25	0.99	0.25

*according to data [44] for Zircaloy-4

**the variance depends on the geometric size of the sample (see Fig. 3), which is determined by the corresponding image size in [42]

Data availability. The MATLAB code is available at: https://github.com/KolesnikMikhail/morphyd

References

1. M. P. Puls. The Effect of Hydrogen and Hydrides on the Integrity of Zirconium Alloy Components. London, Springer-Verlag (2012) 451 p. Crossref
2. M. P. Puls. The Effect of Hydrogen and Hydrides on the Integrity of Zirconium Alloy Components. Hydride Reorientation. Tollered, Sweden, ANT International (2018) 27 p.
3. A. T. Motta et al. J. Nucl. Mater. 518, 440 (2019). Crossref
4. J. S. Bradbrook, G. W. Lorimer, N. Ridley. J. Nucl. Mater. 42, 142 (1972). Crossref
5. O. V. Shiman, M. R. Daymond. Mater. Chem. Phys. 231, 48 (2019). Crossref
6. S. D. Kim, J. S. Kim, J. Yoon. J. Alloys Compd. 735, 2007 (2018). Crossref
7. R. S. Daum, S. Majumdar, Y. Liu, M. C. Billone. J. Nucl. Sci. Technol. 43, 1054 (2006). Crossref
8. M. P. Puls. Metall. Trans. A. 22, 2327 (1991). Crossref
9. J. B. Bai, C. Prioul, D. François. Metall. Mater. Trans. A. 25, 1185 (1994). Crossref
10. A. Gopalan et al. J. Nucl. Mater. 544, 152681 (2021). Crossref
11. J. S. Kim, T. H. Kim, D. H. Kook, Y. S. Kim. J. Nucl. Mater. 456, 235 (2015). Crossref
12. M. C. Billone, T. A. Burtseva, R. E. Einziger. J. Nucl. Mater. 433, 431 (2013). Crossref
13. D. G. Westlake. J. Nucl. Mater. 26, 208 (1968). Crossref
14. K. Une, K. Nogita, S. Ishimoto, K. Ogata. J. Nucl. Sci. Technol. 41, 731 (2004). Crossref
15. J. Li, Z. Wang, H. Wu, G. Chen. J. Nucl. Mater. 537, 152232 (2020). Crossref
16. V. Perovic, G. C. Weatherly, C. J. Simpson. Acta Metall. 31, 1381 (1983). Crossref
17. S. Neogy, D. Srivastava, R. Tewari, R. N. Singh, G. K. Dey, S. Banerjee. J. Nucl. Mater. 322, 195 (2003). Crossref
18. Q. Fang, M. R. Daymond, A. King. Mater. Charact. 134, 362 (2017). Crossref
19. W. Li, S. Hanlon, G. Bickel, A. Buyers, L. Walters, F. Long. J. Nucl. Mater. 539, 152316 (2020). Crossref
20. D. Hardie, M. W. Shanahan. J. Nucl. Mater. 55, 1 (1975). Crossref
21. J. B. Bai, N. Ji, D. Gilbon, C. Prioul, D. François. Metall. Mater. Trans. A. 25, 1199 (1994). Crossref
22. F. Feria, C. Aguado, L. E. Herranz. Ann. Nucl. Energy. 145, 107559 (2020). Crossref
23. A. R. Massih, L. O. Jernkvist. Comput. Mater. Sci. 46, 1091 (2009). Crossref
24. F. Passelaigue, E. Lacroix, G. Pastore, A. T. Motta. J. Nucl. Mater. 544, 152683 (2021). Crossref
25. K. S. Chan. J. Nucl. Mater. 227, 220 (1996). Crossref
26. M. Kolesnik, T. Aliev, V. Likhanskii. Comput. Mater. Sci. 189, 110260 (2021). Crossref
27. T. Aliev, M. Kolesnik, V. Likhanskii, V. Saiutina. J. Nucl. Mater. 557, 153230 (2021). Crossref
28. M. Kolesnik, T. Aliev. Phys. Met. Metallogr. (2023). In press.
29. M. Maric et al. J. Nucl. Mater. 559, 153442 (2022). Crossref
30. R. P. Sear. J. Phys. Condens. Matter. 19, 033101 (2007). Crossref
31. H. I. Aaronson, M. Enomoto, J. K. Lee. Mechanisms of Diffusion Phase Transformations in Metals and Alloys. CRC Press (2010) 667 p.
32. G. J. C. Carpenter. J. Nucl. Mater. 48, 264 (1973). Crossref
33. T. Aliev, M. Kolesnik. J. Phys. Commun. 5, 105005 (2021). Crossref
34. T. Kubo, Y. Kobayashi, H. Uchikoshi. J. Nucl. Mater. 427, 18 (2012). Crossref
35. C. E. Ells. J. Nucl. Mater. 35, 306 (1970). Crossref
36. M. Kolesnik, T. Aliev, V. Likhanskii. J. Nucl. Mater. 508, 567 (2018). Crossref
37. M. Aomi et al. J. ASTM Int. 5, 651 (2008). Crossref
38. M. C. Billone, T. A. Burtseva, Z. Han, Y. Y. Liu. Effects of Multiple Drying Cycles on High-Burnup PWR Cladding Alloys. Aragonne National Laboratory (2014). Available online
39. L. G. Bell, R. G. Duncan. Hydride orientation in Zr-2.5% Nb; how it is affected by stress, temperature and heat treatment. Pinawa, Manitoba, Canada. Atomic Energy of Canada Limited (1975) 31 p.
40. M. Nakatsuka, S. Yagnik. J. ASTM Int. 8, JA102954 (2010). Crossref
41. R. K. Sharma, A. K. Bind, G. Avinash, R. N. Singh, A. Tewari, B. P. Kashyap. J. Nucl. Mater. 508, 546 (2018). Crossref
42. V. M. A. Alvarez, J. R. Santisteban, P. Vizcaino, A. V. Flores, A. D. Banchik, J. Almer. Acta Mater. 60, 6892 (2012). Crossref
43. P. C. A. Simon, C. Frank, L. Q. Chen, M. R. Daymond, M. R. Tonks, A. T. Motta. J. Nucl. Mater. 547, 152817 (2021). Crossref
44. O. Zanellato et al. J. Nucl. Mater. 420, 537 (2012). Crossref
45. R. W. Cahn, P. Haasen. Physical Metallurgy. 4th ed. North-Holland (1996) 4911 p.